ACS APPLIED MATERIALS & INTERFACES

www.acsami.org

Research Article

Ethanol Upgrading to *n*-Butanol Using Transition-Metal-Incorporated Poly(triazine)imide Frameworks

Sabrine M. Cypher, Magnus Pauly, Leslie G. Castro, Carrie L. Donley, Paul A. Maggard,* and Karen I. Goldberg*

Cite This: *ACS Appl. Mater. Interfaces* 2023, 15, 36384−36393

Read Online

ACCESS | Metrics & More | Article Recommendations | Supporting Information

ABSTRACT: The upgrading of ethanol to *n*-butanol was performed using a molecular catalyst integrated into a carbon nitride support, one of the first examples of a supported molecular catalyst performing the Guerbet process. Initial studies using crystalline poly(triazine)imide (PTI) with lithium or transition-metal cations imbedded in the support together with a base as the catalyst system did not produce any significant amounts of *n*-butanol. However, when using the catalyst material formed by treatment of PTI-LiCl with $[(Cp^*)IrCl_2]_2$ (Cp* = pentamethylcyclopentadienyl) along with sodium hydroxide, a 59% selectivity for butanol (13% yield) was obtained at 145 °C. This PTI-(Cp*)Ir material exhibited distinct UV−vis absorption features and powder X-ray diffractions which differ from those of the parent PTI-LiCl and $[(Cp^*)IrCl_2]_2$. The PTI-(Cp*)Ir material was found to have a metal loading of 27% iridium per empirical unit of the framework. Along with the formation of *n*-butanol from the Guerbet reaction, the presence of higher chain alcohols was also observed.

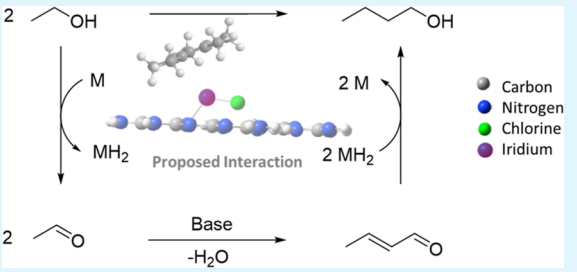

KEYWORDS: *catalysis, Guerbet, ethanol, butanol, carbon nitride, supported catalysts*

INTRODUCTION

Ethanol is a popular fuel additive for conventional gasoline.[1] The reduction of carbon dioxide (CO_2) using renewable energy has the potential to significantly improve the sustainability of ethanol as a fuel, and there are considerable research efforts directed toward this target.[2,3] Yet, ethanol has only 70% of the fuel density of gasoline,[4] and its hygroscopic nature complicates separation techniques and is detrimental to the current engine technology. In contrast, butanol has 90% of the energy density of gasoline and is immiscible with water, which makes it much more desirable as a fuel additive than ethanol.[5−7] Butanol can be added to gasoline at higher concentrations than ethanol (20% vs 10%, respectively), providing an increased ratio of renewable material per gallon of gasoline.[8−10] *n*-Butanol and higher alcohols are also industrially useful chemical feedstocks for solvents, chemical intermediates, and polymers.[8,11]

Recently, increased yields and selectivities for the production of butanol from ethanol using the Guerbet reaction have been reported.[12−16] The Guerbet reaction sequence (Scheme 1) uses a tandem catalyst system to first dehydrogenate ethanol to form acetaldehyde, followed by a base-catalyzed aldol condensation producing crotonaldehyde, and finally hydrogenation of the crotonaldehyde to form *n*-butanol. A variety of homogeneous catalysts have been studied for this transformation.[18−27] Jones et al. were able to achieve 68% butanol selectivity utilizing a $[(PNP)Mn(Br)(CO)_2]$ homogeneous catalyst in neat ethanol,[22] and recently, the Jones group reported a 57% butanol selectivity with [(*p*-cymene)Ru(6,6′-bpy^{OH})Cl]Cl as their catalyst in an aqueous solvent system.[25] A variety of heterogeneous catalysts for the Guerbet process involving commercial cobalt powder,[28] metal oxides,[29−36] metal−organic frameworks,[37] and hydroxyapatite[38−40] have also been reported with butanol selectivities of 70, 50, 99, and 75%, respectively. In a recent report, a homogeneous (NNN) Ru pincer catalyst was used to obtain 62% ethanol conversion

Scheme 1. Upgrading of Ethanol to *n*-Butanol via the Guerbet Process

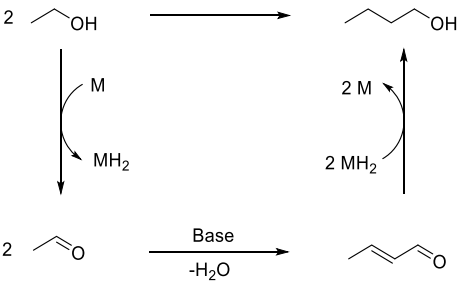

Received: May 23, 2023
Accepted: June 30, 2023
Published: July 24, 2023

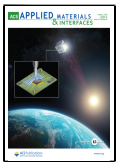

with a 45% yield of n-butanol. When a modified NNN ligand was used to anchor the Ru catalyst to a support, a 27% butanol yield with 35% conversion was achieved (77% selectivity).[41] Unfortunately, it was not possible to recycle the supported catalyst. Overall, in catalytic systems for ethanol upgrading to butanol, although higher selectivities for butanol are often observed with heterogeneous catalysts, conversion rates are typically much lower (~15% for heterogeneous versus ~50% for homogeneous), and heterogeneous systems operate at higher temperatures than homogeneous (170−250 °C for heterogeneous versus 145 °C for homogeneous).

In this contribution, we report our efforts to combine the benefits of heterogeneous catalysts (robust and easy to separate after reaction) with homogeneous catalysis (greater tunability of the active site to increase selectivity and efficiency) by integrating transition-metal salts and organometallic compounds into a heterogeneous organic framework. We have targeted the poly(triazide)imide (PTI) carbon nitride framework (Figure 1, PTI-LiCl), taking advantage of the reported robust synthetic procedure to produce a uniform crystalline two-dimensional network with LiCl templated in the pockets of the framework.[42] Carbon nitrides have also been used as a support to perform hydrogenation reactions[43,44] but have not yet been applied to the Guerbet reaction. Similar two-dimensional materials are used for electron transports,[45] and the effects of chemical alterations to the surfaces of these materials have been examined with respect to the electronics and reactivity of the materials.[46−48] The presence of removable Li^+ cations in the framework of PTI-LiCl also provides access to PTI materials with other metal cations which could further be probed for catalytic activity. Finally, carbon nitrides are known to have photocatalytic[49−52] and electrocatalytic[53] properties, and thus, this 2-D framework may be amenable to be incorporated with semiconductors in the future.

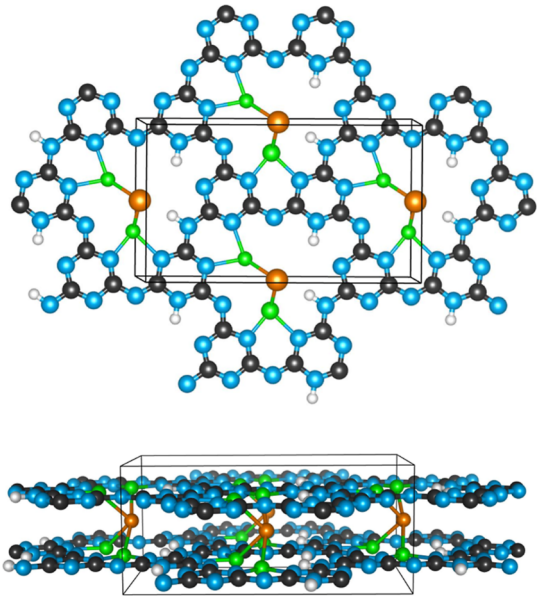

Figure 1. Crystalline structure of PTI-LiCl ($C_6N_9H_2Li_2Cl$) from the top (top) and side (bottom) views. The framework is a 2-dimensional sheet of carbon (black) and nitrogen (blue) with hydrogens (white) residing on some of the nitrogen. Within the pocket lie the lithium (green) atoms which interact with the nitrogens of the triazine. The charge-balancing chloride (orange) resides between the layers of the framework as shown in the side view.

In this study, the parent PTI-LiCl along with a variety of carbon nitride materials formed by replacing the Li^+ ions with transition-metal cations were explored as catalysts for the ethanol Guerbet reaction to produce butanol. A series of homogeneous pre-catalysts were also integrated into the PTI-LiCl material, and the catalytic activity of these new materials for the Guerbet reaction was investigated.

RESULTS AND DISCUSSION

Reactivity Studies of PTI-LiCl. Initial experiments were carried out to assess the reactivity of the parent material PTI-LiCl as a catalyst for ethanol conversion to butanol. PTI-LiCl, potassium *tert*-butoxide, and neat ethanol were added to a sealable, pressure vessel and heated at 145 °C for 24 h. Approximately 10% of the ethanol was consumed by the reaction, but no butanol formation (<1% yield) was observed. A variety of bases and base loadings were probed, but none of these alterations improved the performance of the catalyst system (Table S7). A control reaction of heating just ethanol yielded no conversion of ethanol, whereas ethanol with NaOH showed ~7% consumption of ethanol with only trace butanol formation (Table S7). Gas chromatography (GC) analysis did not reveal formation of any esters (e.g., ethyl acetate) produced from the side reactions illustrated in Scheme 2.[54−56]

Formation and Reactivity of PTI-MCl. PTI frameworks with transition-metal ions displacing *x* number of Li^+ were then probed. Table 1 shows the ratio of metal per pocket of the carbon nitride framework (as determined by elemental analysis) for each material tested. PTI-MCl, potassium *tert*-butoxide, and neat ethanol were heated together at 145 °C for 24 h. For materials loaded as M = Fe(II), Co(II), Mn(II), or Zn(II), around 2−10% conversion of ethanol was observed but no substantial *n*-butanol formation (<1% yield) (Table S8). Again, no other byproducts were detected via GC analysis or ^{1}H NMR spectroscopy. Using the Ru(II) material, PTI-RuCl

Scheme 2. Possible Side Reactions during Ethanol Upgrading

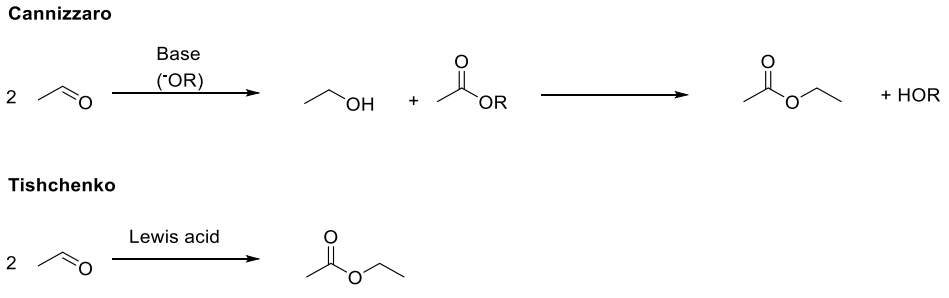

https://doi.org/10.1021/acsami.3c07396
ACS Appl. Mater. Interfaces 2023, 15, 36384−36393

Table 1. Metal Loading of the PTI Framework ($C_6N_9M_xCl_2$) with Li^+ Displaced by Various Transition Metals

transition metal	metal loading per empirical formula unit
Fe	0.4
Co	0.25
Mn	0.5
Zn	0.7
Ru	0.08

resulted in a 14% conversion of ethanol with a 4% yield of butanol (Table S8). A variety of homogeneous compounds with Ru metal centers have been reported as active hydrogenation catalysts.[25,57,58] The surprisingly similar reactivity exhibited by the parent PTI-LiCl and most of the transition-metal-exchanged PTI materials showed that integrating only the transition metal into the pocket of the PTI framework did not produce effective catalysts for the Guerbet reaction. To build a heterogeneous analogue more similar to the homogeneous catalysts previously studied for Guerbet reactions,[18,20,21,25] organometallic complexes were next incorporated into the PTI framework.

Incorporation of Homogeneous Catalysts into PTI-LiCl. A range of homogeneous metal compounds in combination with PTI were also explored as catalysts for the conversion of ethanol to butanol. The strategy of immobilizing homogeneous catalysts onto heterogeneous supports has been used to promote a variety of reactions. For example, hydrogenation reactions have been reported with homogeneous catalysts supported on silica,[59] CO_2 reduction with catalysts on carbon,[60,61] and cross-coupling catalysts in a silica matrix.[62] Four different molecular complexes which are known precursors to homogeneous hydrogenation catalysts were supported on PTI-LiCl and used in the study of the Guerbet reaction. Samples of $[(Cp^*)IrCl_2]_2$ (Cp^* = pentamethylcyclopentadienyl), $[(Cp^*)RhCl_2]_2$, $[(p\text{-cymene})RuCl_2]_2$ (*p*-cymene = 4-isopropyltoluene), and $[(C_6Me_6)RuCl_2]$ (C_6Me_6 = hexamethylbenzene) (Figure 2) were each integrated into separate samples of the PTI host. To integrate the materials, the parent PTI-LiCl was sonicated in acetonitrile for an hour, then the respective homogeneous dimer was added, and sonication was continued for an additional hour. The resulting solutions were evaporated in vacuo and washed with benzene

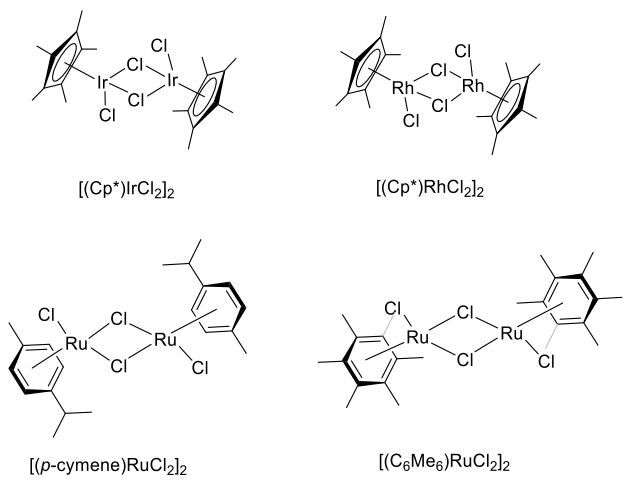

Figure 2. Homogeneous precursors which were tested for integration with PTI-LiCl.

to remove any excess homogeneous material. In contrast to the white powder of PTI-LiCl, the incorporation of the homogeneous compounds yielded pale-colored powders (yellow for the Ir material, orange for the Rh material, and reddish-orange for both Ru materials).

Characterization of PTI-(arene)M Materials. The colored powders of the PTI-LiCl/homogeneous catalyst materials were analyzed by UV−vis spectroscopy. Figure 3 shows that the PTI-(Cp*)Ir material exhibits an absorbance feature at 337 nm similar to the starting dimeric material $[(Cp^*)IrCl_2]_2$ (333 nm), but PTI-(Cp*)Ir has an additional absorbance at 289 nm. It is interesting to compare the data to a UV−vis spectrum of [(Cp*)Ir(bpy)Cl]Cl (bpy = bipyridine), also shown in Figure 2, which shows a strong absorbance at 293 nm. The similarity in the 293 nm absorbance could be indicative of the Ir center having a binding interaction with nitrogens inside the pocket of PTI analogous to the binding of Ir to bpy in [(Cp*)Ir(bpy)Cl]Cl. In contrast, the PTI-LiCl material with the Ru and Rh complexes only exhibited the absorbance features of the dimeric starting materials. For example, PTI-(*p*-cymene)Ru has absorbance features at 336 and 418 nm which resemble the dimeric molecular species with absorbance features at 337 and 421 nm. There is no indication of a new absorbance feature similar to the 292 nm absorbance evident in the bpy derivative, [(*p*-cymene)Ru-(bpy)Cl]Cl. The PTI-(Cp*)Rh material has absorbance features at 270 and 409 nm which match the $[(Cp^*)RhCl_2]_2$ absorbance spectra with absorbance features at 270 and 406 nm. PTI-(C_6Me_6)Ru showed observed absorbance at 343 and 424 nm which align well with the absorbance feature of the dimeric $[(C_6Me_6)RuCl_2]_2$ (341 and 424 nm). There is no evidence of any absorbance similar to those of the bipyridyl analogue, [(C_6Me_6)Ru(bpy)Cl]Cl (293 and 362 nm). Overall, the evidence suggests that the (Cp*)Ir experiences some covalent binding of the metal center to the PTI framework, while the dimeric starting material species remain partially intact in its interaction with the PTI network for Ir and fully intact for the Ru and Rh complexes.

Powder X-ray diffraction data of the catalyst-integrated PTI-LiCl materials (Figure 4) each showed diffraction peaks that could be indexed to its basic crystalline structure in the orthorhombic crystal system (a = 14.6 Å; b = 8.6 Å; c = 6.7 Å). For example, PTI-(C_6Me_6)Ru showed predominantly strong diffraction peaks corresponding to PTI-LiCl. No evidence was found for the incorporation of the molecular catalyst as part of its bulk crystalline structure. In PTI-(*p*-cymene)Ru, additional, unidentified, weak diffraction peaks are observed together with weaker diffraction peaks for crystalline PTI-LiCl, suggesting that either two separate phases are present or that a reaction has occurred to give a more amorphous material. For the Cp* metal−organic species, diffraction peaks for crystalline PTI-LiCl are again observed together with additional, unidentified diffraction peaks for both Cp* materials. PTI-(Cp*)Ir is unique, in that weak diffraction peaks of $[(Cp^*)IrCl_2]_2$ can be observed in addition to PTI-LiCl (Figure S1). The observation of $[(Cp^*)IrCl_2]_2$ in PTI-(Cp*)Ir supports the hypothesis that the basic crystalline structure of PTI-LiCl is being maintained, with the additional diffraction peaks likely resulting from the co-crystallization of the molecular catalysts (in excess) upon drying.

X-ray photoelectron spectroscopy (XPS) data was also collected on these materials (see Figures S2−S9 and Tables S1−S4). The empirical formula of PTI-LiCl was determined to

https://doi.org/10.1021/acsami.3c07396
ACS Appl. Mater. Interfaces 2023, 15, 36384−36393

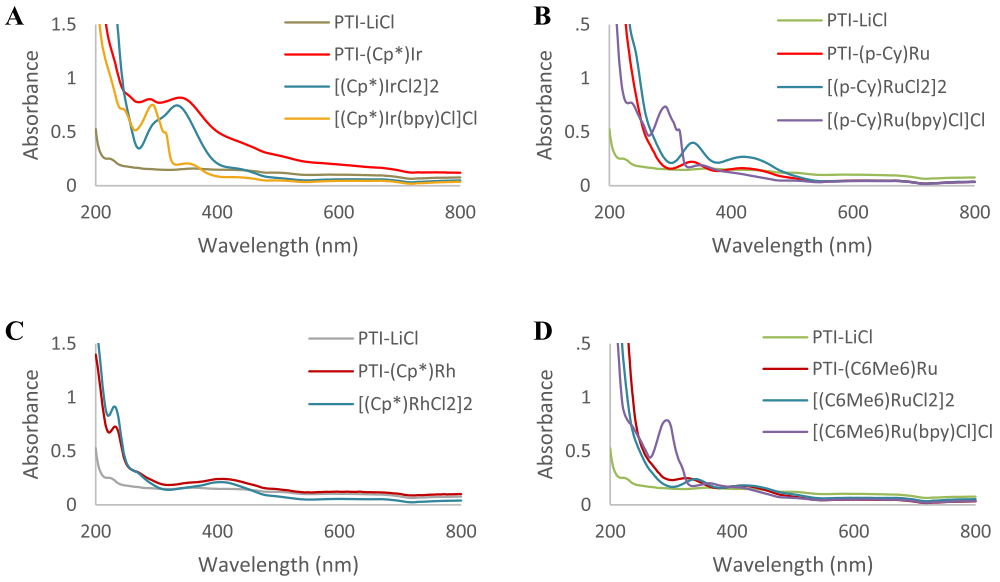

Figure 3. UV−vis spectra after sonication of the molecular catalyst with PTI framework suspended in acetonitrile and filtered through PTFE. p-Cy = *p*-cymene. Absorbance spectra of (Cp*)Ir compounds (**A**), (*p*-cymene)Ru compounds (**B**), (Cp*)Rh compounds (**C**), and (C_6Me_6)Ru compounds (**D**).

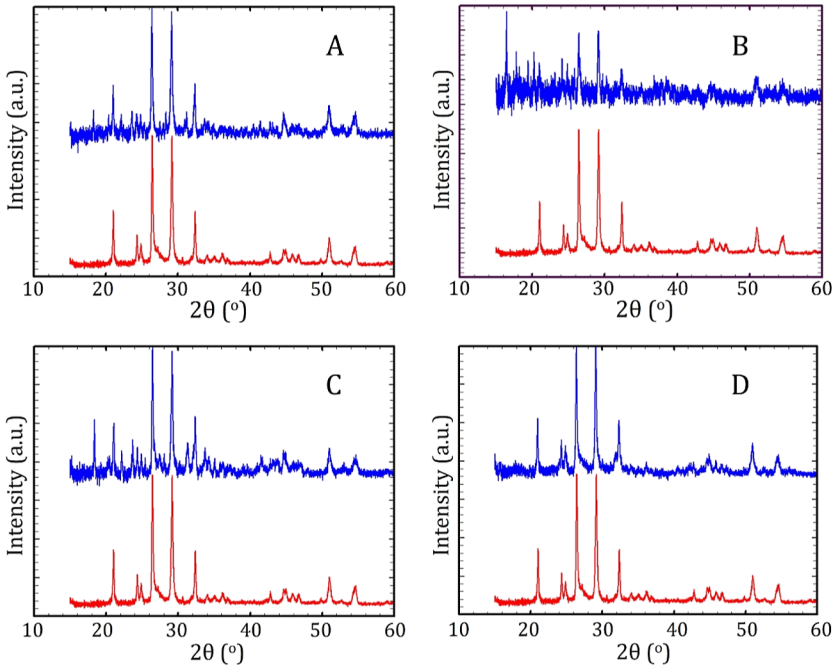

Figure 4. Powder X-ray diffraction spectra of molecular catalyst-integrated PTI materials: PTI-(Cp*)Ir (**A**), PTI-(*p*-cymene)Ru (**B**), PTI-(Cp*)Rh (**C**), and PTI-(C_6Me_6)Ru (**D**). p-Cy = *p*-cymene. The blue trace is the PTI-(arene)M material, and the red trace is PTI-LiCl. An extra 100 units deducted from the intensity values of PTI-LiCl to offset the spectra for comparison.

be $C_6N_9H_2Li_2Cl$ from elemental analysis.[42] Therefore, the atomic ratio of Li/N in PTI-LiCl is 2:9 or 0.22. The ratio of Li/N for each of the molecularly integrated materials as measured by XPS was found to be 0.13 for PTI-(Cp*)Ir, 0.07 for PTI-(Cp*)Rh, 0.22 for PTI-(*p*-cymene)Ru, and 0.20 for PTI-(C_6Me_6)Ru. These data suggest that for the case of the two Cp* compounds, a large portion of the Li^+ have been displaced from the material, but PTI-(*p*-cymene)Ru and PTI-(C_6Me_6)Ru contained a similar amount of Li compared to the parent PTI-LiCl. XPS analysis was consistent with Ir(III), Rh(III), and Ru(II) oxidation states.[63] Based on the atomic concentrations of the metals present in the materials (the M/N ratio), the metal loading per pocket of each of these materials was found to be 27% Ir in PTI-(Cp*)Ir, 90% Rh in PTI-(Cp*)Rh, 36% Ru in PTI-(*p*-cymene)Ru, and 9% Ru in PTI-(C_6Me_6)Ru (see the Supporting Information). For PTI-(Cp*)Ir, the data is consistent with 27% of the pockets in the PTI framework containing an Ir atom. Inductively coupled plasma mass spectroscopy (ICP−MS) was also performed on the PTI-(arene)M materials (Table S6). Most of the materials showed a higher ratio of Li/M with ICP than with XPS. ICP involves digesting the material in acidic conditions, whereas XPS is a surface technique. This difference suggests that the metal present in the bulk material may be lower so that the

https://doi.org/10.1021/acsami.3c07396
ACS Appl. Mater. Interfaces 2023, 15, 36384−36393

Table 2. Guerbet Reactivity of Integrated PTI Materials versus Molecular Dimers Both with and without the Presence of PTI-LiCl[a]

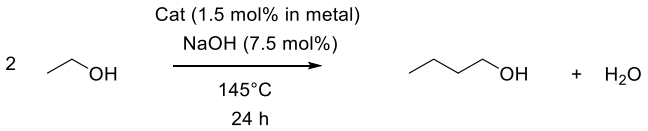

Entry	Catalyst	Conversion (%)	Yield *n*BuOH (%)	Yield Higher Alcohols[b] (%)	Selectivity[c] (%)
1	PTI-(Cp*)Ir	22(3)	13(0)	6(3)	59(7)
2	$[Ir(Cp^*)Cl_2]_2$	32(5)	13(2)	11(1)	41(8)
3	$[Ir(Cp^*)Cl_2]_2$ + PTI-LiCl	51(3)	12(0)	11(0)	23(1)
4	[(Ir(Cp*)(bpy)Cl]Cl	26(9)	10(1)	3(0)	41(10)
5	PTI-(*p*-cymene)Ru	28(2)	5(0)	2(0)	17(0)
6	$[Ru(p\text{-cymene})Cl_2]_2$	52(3)	2(0)	1(0)	4(0)
7	$[Ru(p\text{-cymene})Cl_2]_2$ + PTI-LiCl	69(3)	2(0)	1(0)	3(0)
8	PTI-(Cp*)Rh	20(9)	3(0)	1(0)	20(9)
9	$[Rh(Cp^*)Cl_2]_2$	28(9)	3(1)	2(0)	14(7)
10	$[Rh(Cp^*)Cl_2]_2$ + PTI-LiCl	22(4)	4(0)	2(0)	20(4)
11	PTI-(C_6Me_6)Ru	39(1)	2(0)	0.6(1)	6(0)
12	$[Ru(C_6Me_6)Cl_2]_2$	40(5)	2(0)	0.5(1)	4(1)
13	$[Ru(C_6Me_6)Cl_2]_2$ + PTI-LiCl	43(8)	3(1)	0.8(2)	6(2)

[a]Carbon nitride material (2.0 mg), NaOH (0.5 mmol), and dried ethanol (6.7 mmol) were loaded into a custom 5 mL reaction-grade borosilicate Schlenk tube with a Teflon pin. The vessel was sealed and heated at 145 °C in an aluminum block for 24 h. Average of two trials. [b]Higher alcohols = 2-ethylbutanol, 1-hexanol, 2-ethylhexanol, and 1-octanol. [c]Selectivity = (moles of *n*-butanol produced)/(moles of ethanol consumed/2) × 100.

metal compounds may only be present on the outer layers of the PTI-LiCl material. The only exception to this was PTI-(Cp*)Rh which had a similar Li/M ratio measured in both techniques (0.67 and 0.73).

Reactivity Studies of PTI-(arene)M Materials. The activity of these new molecular-PTI species as catalysts for the Guerbet reaction to upgrade ethanol to butanol was investigated. Reactions were performed with (1) the integrated PTI materials, (2) homogeneous molecular dimers, and (3) mixtures of molecular dimer and PTI-LiCl (Table 2). Heating PTI-(Cp*)Ir in neat ethanol with sodium hydroxide at 145 °C for 24 h (entry 1) led to a 22% conversion of the ethanol. An *n*-butanol yield of 13% was determined by GC analysis along with a 6% total yield of higher alcohols (e.g., 2-ethylbutanol, 1-hexanol, 2-ethylhexanol, and 1-octanol). Thus, a 59% selectivity for butanol was observed. By comparison in entry 2, the $[(Cp^*)IrCl_2]_2$ proceeded with a higher conversion of ethanol (32%) with a similar yield of 13% for butanol. A larger amount of higher alcohols was also observed (11%), resulting in a butanol selectivity of 41%. As shown in entry 3, the mixing of PTI-LiCl with the homogeneous $[(Cp^*)IrCl_2]_2$ produced similar yields of butanol and higher alcohols (12 and 11%, respectively) to the results with only homogeneous dimers. However, a significantly higher conversion of ethanol was observed (51%). Similar to the ethanol reactions with the parent PTI-LiCl, there was missing ethanol in the product mixture (10−30% for entries 1−3). Previously reported studies on homogeneous Guerbet reactions range from 5 to 40% missing ethanol.[17−22,24,26] It is noted that the reactions without the integrated PTI/homogenous catalyst had significantly higher amounts of unaccounted-for ethanol. PTI-Cp*Ir was analyzed post-catalysis and the material remained intact (Figure S2). Due to the UV−vis absorbance spectra of PTI-(Cp*)Ir suggesting that the Ir center may be interacting with the pocket of the PTI framework, [(Cp*)Ir(bpy)Cl]Cl was tested for Guerbet reactivity (entry 4) and showed lower butanol yields (10% vs 13%), but the conversion and selectivity were similar to the those of the $[(Cp^*)IrCl_2]_2$ trial. PTI-(*p*-cymene)Ru (entries 5−7) also exhibits better reactivity than the starting dimer both with and without the presence of PTI-LiCl as seen by the butanol selectivity of 17% vs 3% or 4%. Both PTI-(Cp*)Rh (entries 8−10) and PTI-(C_6Me_6)Ru (entries 11−13) showed similar reactivity (butanol selectivities 20 and 6%, respectively) to their respective molecular dimers which suggested that these materials do not successfully bind or interact with the bulk PTI-LiCl material.

Using the best-performing material from the initial screen (Table 2), PTI-(Cp*)Ir experiments with different bases were carried out (Table 3). Notably in entry 1 of Table 3 when no base was added, no product formation occurred, and all ethanol was still present after heating. As can be seen in entry 2 of Table 3, sodium hydroxide was the best-performing additive with an *n*-butanol selectivity of 59%. While the reaction with sodium *tert*-butoxide (entry 3) proceeded to higher conversion, a lower *n*-butanol selectivity of 39% resulted. Potassium *tert*-butoxide and sodium ethoxide (entries 4 and 7) showed similar selectivity for *n*-butanol of about 30%. There was a further drop-off of selectivity using potassium hydroxide or sodium methoxide (entries 5 and 6) which provided 21 and 19% selectivity, respectively. Most notably, the yield of *n*-butanol for these additives was all the same with minor variations of the ethanol conversion being responsible for any variance in the selectivity. The presence of *tert*-butanol was observed as a product when the *tert*-butoxide salts were employed. Water formed during the reaction can react with the butoxide salt to give the corresponding alcohol *tert*-butanol. Similarly, the presence of methanol was observed in reactions with sodium methoxide. The use of cesium hydroxide

https://doi.org/10.1021/acsami.3c07396
ACS Appl. Mater. Interfaces 2023, 15, 36384−36393

Table 3. Guerbet Reactivity of the Integrated PTI-(Cp*)Ir Material with Various Base Additives[a]

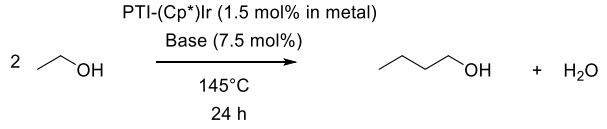

entry	base	conversion (%)	yield *n*BuOH (%)	yield higher alcohols[b] (%)	selectivity[c] (%)
1	None	0(0)	0(0)	0(0)	0(0)
2	NaOH	22(3)	13(0)	6(3)	59(7)
3	NaO^{t}Bu[d]	34(9)	13(2)	6(4)	39(4)
4	KO^{t}Bu[d]	29(3)	9(1)	6(1)	33(1)
5	KOH	14(3)	3(1)	2(1)	21(4)
6	NaOMe[e]	44(4)	8(1)	6(2)	19(0)
7	NaOEt	24(2)	12(1)	6(0)	35(4)
8	CsOH·H2O	24(3)	5(0)	1(0)	20(2)
9	$2Al(OH)_3$	44	0	0	0

[a]Carbon nitride material (2.0 mg), base (0.5 mmol), and dried ethanol (6.7 mmol) were loaded into a custom 5 mL reaction-grade borosilicate Schlenk tube with a Teflon pin. The vessel was sealed and heated at 145 °C in an aluminum block for 24 h. Average of two trials. [b]Higher alcohols = 2-ethylbutanol, 1-hexanol, 2-ethylhexanol, and 1-octanol. [c]Selectivity = (moles of *n*-butanol produced)/(moles of ethanol consumed/2) × 100. [d]The presence of *tert*-butanol was observed. [e]The presence of methanol was observed.

monohydrate (entry 8) lowered the activity further (20% selectivity), suggesting that the cation may have some importance for the aldol condensation step of the Guerbet process, but the significance does not extend to the smaller ions of sodium and potassium. Aluminum hydroxide (entry 9) was also tested, but no reaction was observed due to poor solubility. Thus, sodium hydroxide was the best-performing base additive.

Issues with the reproducibility of butanol selectivity with sodium hydroxide were observed over the duration of this study. For a given batch of PTI-(Cp*)Ir, reactions run in parallel could give ranges from 30 to 65% butanol selectivity. Due to this observation, further optimization reactions were performed using potassium *tert*-butoxide as the selectivity observed was more consistent from batch to batch of PTI-(Cp*)Ir. Variable base loadings were also evaluated (Table 4) to better compare to the homogeneous Guerbet reactions which range in base loadings: 5% with Wass's (*p*-cymene)Ru catalyst,[19] 10% with Kumar's (NNN)Ru catalysts,[16] 25% for Jones' (PNP)Mn,[22] 40% with Szymczak's (NNN)Ru catalyst,[27] and 200% with Wass's (PNP)Re or (PP)Mn catalysts.[24,26] As the amount of added KO^{t}Bu was increased from 3.5 to 25%, there was a slight increase in selectivity (from 25 to 34%) but the error increased at higher loadings. The effect of base loading seemed minimal when above 7.5% base loading. These data along with the lack of observation of the aldehyde intermediates in any of the reactions further suggest that the dehydrogenation of ethanol was the slowest step of the Guerbet reaction (Scheme 1) as previously proposed for homogeneous Guerbet catalysts.[23]

The reaction condition variables of temperature (Table 5) and time (Table 6) were also evaluated. Upon dropping the temperature of the reaction from 145 to 120 °C, there was no significant change to the *n*-butanol selectivity (entries 1 and 2). Further temperature decreases to 100 and 80 °C led to a slight uptick in selectivity from 28 to 38% (entries 3 and 4), though

Table 4. Guerbet Reactivity of the Integrated PTI-(Cp*)Ir Material with Various Loadings of KO^{t}Bu[a]

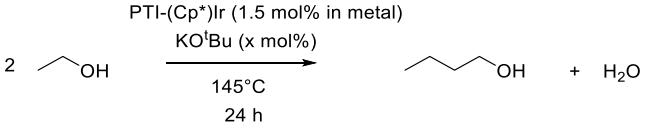

entry	base loading (mol %)	conversion (%)	yield *n*BuOH (%)	yield higher alcohols[b] (%)	selectivity[c] (%)
1	3.5	30(3)	7(1)	6(1)	25(1)
2	7.5	29(3)	9(1)	6(1)	33(1)
3	12.5	39(9)	10(0)	6(1)	28(7)
4	25	50(5)	17(1)	7(1)	34(6)

[a]Carbon nitride material (2.0 mg), KO^{t}Bu (0.25, 0.5, 1, and 2 mmol), and dried ethanol (6.7 mmol) were loaded into a custom 5 mL reaction-grade borosilicate Schlenk tube with a Teflon pin. The vessel was sealed and heated at 145 °C in an aluminum block for 24 h. Average of two trials. [b]Higher alcohols = 2-ethylbutanol, 1-hexanol, 2-ethylhexanol, and 1-octanol. [c]Selectivity = (moles of *n*-butanol produced)/(moles of ethanol consumed/2) × 100. The presence of *tert*-butanol was observed.

Table 5. Guerbet Reactivity of the Integrated PTI-(Cp*)Ir Material at Various Reaction Temperatures[a]

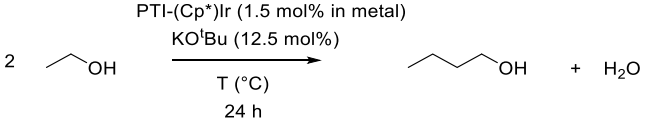

entry	*T* (°C)	conversion (%)	yield *n*BuOH (%)	yield higher alcohols[b] (%)	selectivity[c] (%)
1	145	39(9)	10(0)	6(1)	28(7)
2	120	32(4)	9(2)	8(3)	28(3)
3	100	21(1)	7(1)	7(1)	35(1)
4	80	11(2)	4(1)	2(0)	38(8)

[a]Carbon nitride material (2.0 mg), KO^{t}Bu (1 mmol), and dried ethanol (6.7 mmol) were loaded into a custom 5 mL reaction-grade borosilicate Schlenk tube with a Teflon pin. The vessel was sealed and heated at the given temperature in an aluminum block for 24 h. Average of two trials. [b]Higher alcohols = 2-ethylbutanol, 1-hexanol, 2-ethylhexanol, and 1-octanol. [c]Selectivity = (moles of *n*-butanol produced)/(moles of ethanol consumed/2) × 100. The presence of *tert*-butanol was observed.

the yield of *n*-butanol slowly decreased as the temperature was lowered. Though there was a minor improvement to the selectivity at lower temperatures, the impact on conversion and butanol yield mitigates this benefit. An increase in the reaction time from 24 to 48 h showed no change in butanol yield (10% vs 11%) (entries 1 and 2, Table 6) or selectivity (28% vs 29%). There was an increase in conversion (28% vs 37%). The additional time did not seem to increase the amount of upgrading beyond butanol (i.e., no significant increase in higher alcohols formed) either. Overall, there was no increase in reactivity past 24 h, suggesting that the catalyst system was no longer functioning. Shortening the reaction time to 14 h showed no drop in butanol yield (12%) (entry 3). However, when the reaction time was dropped to just 4 h, the yield of butanol was lower (7%). Though entry 4 shows further improvement of the selectivity to up to 52%, the reaction was not complete at this point.

The addition of extraneous water was also investigated to verify to what extent water may hinder the reaction. Since

https://doi.org/10.1021/acsami.3c07396
ACS Appl. Mater. Interfaces 2023, 15, 36384−36393

Table 6. Guerbet Reactivity of the Integrated PTI-(Cp*)Ir Material at Various Reaction Times[a]

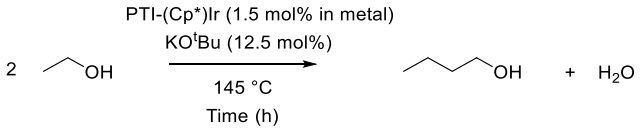

entry	time (h)	conversion (%)	yield *n*BuOH (%)	yield higher alcohols[b] (%)	selectivity[c] (%)
1	24	28(2)	10(1)	6(1)	35(3)
2	48	37(1)	11(0)	6(0)	29(1)
3	14	29(4)	12(1)	10(1)	43(6)
4	4	12(1)	7(0)	4(0)	52(1)

[a]Carbon nitride material (2.0 mg), KO^{t}Bu (1 mmol), and dried ethanol (6.7 mmol) were loaded into a custom 5 mL reaction-grade borosilicate Schlenk tube with a Teflon pin. The vessel was sealed and heated at 145 °C in an aluminum block for the given amount of time. Average of two trials. [b]Higher alcohols = 2-ethylbutanol, 1-hexanol, 2-ethylhexanol, and 1-octanol. [c]Selectivity = (moles of *n*-butanol produced)/(moles of ethanol consumed/2) × 100. The presence of *tert*-butanol was observed.

water is a byproduct of the Guerbet reaction, a detrimental effect of water could explain why the efficiency of the system declines over time. First, a sub-stoichiometric amount of water was added (Table 7, entry 2). The temperature of the reaction was dropped to 120 °C to accommodate the additional vapor pressure from another volatile reagent. The ethanol conversion, yield of *n*-butanol, yield of higher alcohols, and selectivity all dropped with the addition of water. Added water was increased to 1 equiv compared to ethanol (Table 7, entry 3), and this change further inhibited the reaction as exhibited by the additional decrease in conversion and yields. Overall, these results suggest that water has an inhibitory role in the reaction, providing an explanation for the relatively low conversion rates across all reaction conditions examined. This inhibition by water also explains the decline of catalytic activity at longer reaction times as water is a byproduct of the reaction.

Table 7. Guerbet Reactivity of the Integrated PTI-(Cp*)Ir Material with Extraneous Water Present[a]

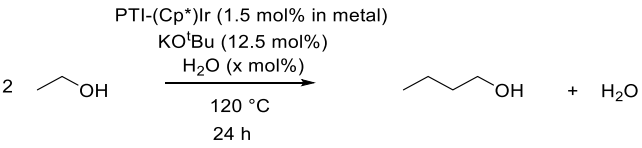

entry	water added (equiv)	conversion (%)	yield *n*BuOH (%)	yield higher alcohols[b] (%)	selectivity[c] (%)
1	0	32(4)	9(2)	8(3)	28(3)
2	0.25	22(2)	6(1)	3(0)	26(0)
3	1	12(4)	3(1)	1(0)	22(7)

[a]Carbon nitride material (2.0 mg), KO^{t}Bu (1 mmol), dried ethanol (6.7 mmol), and water (0, 1.5, or 6.7 mmol) were loaded into a custom 5 mL reaction-grade borosilicate Schlenk tube with a Teflon pin. The vessel was sealed and heated at 120 °C in an aluminum block for the given amount of time. Average of two trials. [b]Higher alcohols = 2-ethylbutanol, 1-hexanol, 2-ethylhexanol, and 1-octanol. [c]Selectivity = (moles of *n*-butanol produced)/(moles of ethanol consumed/2) × 100.

We further probed the recycling capabilities of PTI-Cp*Ir and found that the yield of butanol decreased with repeat cycles illustrating that this system was not yet optimized for recyclability (Figures S13 and S14). We employed two methods for recycling: (1) evaporation of volatiles and then reloading with fresh ethanol and (2) filtration of solution and then reloading with fresh ethanol. There was a greater decrease observed with the filtration method, suggesting that the molecular catalyst may not be tightly bound in the carbon nitride framework. This highlights the importance of catalyst attachment for its separation and re-use in a commercial-type process. Since this is not an optimized fixed bed system, this proof-of-concept of integrating molecular catalysts with supports demonstrates its strong potential merit. Additional studies, such as more robust attachment strategies, can be explored with larger scaled-up systems.

Fourier transform infrared (FTIR) spectroscopy of the post-catalysis PTI-(Cp*)Ir revealed that with the presence of NaOH, formation of C−H bonds were observed on the PTI material (Figure S15). Since the parent PTI does not contain any C−H bonds, these must be formed during the reaction. Base-catalyzed C−N coupling is precedented.[64,65] This side reaction may account for some of the missing ethanol that was observed in our reactions; however, due to the small material loading (2 mg), we do not expect this to be a major contribution to ethanol consumption.

CONCLUSIONS

Herein, new materials were fabricated for use as catalysts in the Guerbet reaction by incorporating the molecular species $[(Cp^*)IrCl_2]_2$ into the PTI carbon nitride framework. This system is one of the first to use a supported molecular catalyst for Guerbet catalysis. The effect of base additive, base loading, reaction time, reaction temperature, and addition of extraneous water was evaluated. This new PTI-(Cp*)Ir material with sodium hydroxide as the base additive achieved 59% butanol selectivity (145 °C, 24 h). This observed selectivity is similar to that reported for homogenously catalyzed reactions,[21,22] suggesting that the integrated catalyst behaves in a similar manner to the homogeneous Guerbet systems. However, the ethanol conversion (22%) is lower than these homogeneous systems (30−60%). In 2016, Cao et al.[66] presented a figure detailing the ethanol conversion vs butanol selectivity of a variety of catalytic Guerbet systems. With a 59% butanol selectivity and 22% ethanol conversion, our system would appear in the same region as the reported heterogeneous liquid-phase systems. Furthermore, a similar level of selectivity (52%) can be achieved using PTI-(Cp*)Ir with KO^{t}Bu (145 °C, 4 h), though the overall production in this case is lower (7% butanol yield vs 13% with NaOH at 24 h). The reaction with PTI-(Cp*)Ir, however, was found to be inhibited by water which is a byproduct of the Guerbet reaction, limiting ethanol conversions (~20 to 30%) and butanol yields (~10%). Studies are underway to further modify (a) the molecular catalyst species by introducing hydroxide or other polar groups for better water tolerance and (b) the PTI framework by the addition of molecular dopants with tunable functional groups during crystallization to better optimize the yields. Furthermore, the carbon nitride framework presents the potential for the reaction to be incorporated into an electrochemical or photochemical process in the future.

https://doi.org/10.1021/acsami.3c07396
ACS Appl. Mater. Interfaces 2023, 15, 36384−36393

EXPERIMENTAL SECTION

General. Reagents were obtained from the following sources: sodium hydroxide, potassium hydroxide, aluminum hydroxide, and diethyl ether (Fisher Chemical); sodium *tert*-butoxide, potassium *tert*-butoxide, *n*-butanol, 2-ethylbutanol, 2-ethylhexanol, and 1-octanol (Sigma-Aldrich); ethanol (200 proof, anhydrous) (Decon Laboratories, Inc.); and 1,4-dioxane (99+%, stabilized) (Acros). Sodium methoxide and sodium ethoxide were synthesized following the literature procedure.[67,68] Ethanol was dried over calcium hydride, distilled, and stored over 4 Å molecular sieves in a nitrogen glovebox. Diethyl ether was dried by passage through activated alumina and molecular sieve columns under an argon flow (a Grubb's type solvent purification system by JC Meyer Solvent Systems). PTI-LiCl and organometallic materials were synthesized according to the literature: PTI-LiCl,[42] $[(Cp^*)IrCl_2]_2$,[69] $[(Cp^*)RhCl_2]_2$,[69] $[(p\text{-cymene})RuCl_2]_2$,[70] and $[(C_6Me_6)RuCl_2]_2$.[70] Gas chromatograms were recorded on an Agilent Technologies 7890A gas chromatograph with an autoinjector, a FID, and a DB-FFAP column (30 m × 0.25 mm ID × 0.25 μm). Carrier gas: Helium. Method used: starting oven temperature of 40 °C (hold for 4 min), then heated to 240 °C at 30 °C/min; column pressure: 19.4 psi, total flow: 105 mL/min, column flow: 2 mL/min, split ratio: 50, and linear velocity: 40 cm/s.

Integration of Molecular Catalysts with PTI-LiCl. PTI-LiCl (30 mg, 0.12 mmol) was first suspended in acetonitrile (1.5 mL) in a 1-dram vial and sonicated for an hour. The desired molecular dimer (0.06 mmol) was then added, and the solution was further sonicated for an additional hour. The suspended mixture was evaporated on a rotary evaporator to a thin-layer coat on the interior of the vial. The residue was washed with excess benzene until the washings became clear. The material was then dried overnight in vacuo.

General Procedure for the Guerbet Reaction. Carbon nitride material (2.0 mg), base (0.5 mmol), and dried ethanol (6.7 mmol) were loaded into a custom 5 mL reaction-grade borosilicate Schlenk tube with a Teflon pin inside a nitrogen-filled glovebox. The vessel was sealed and heated at 145 °C in an aluminum block for 24 h. **Safety Note**: the vapor pressure of ethanol at 145 °C is 9 atm. All reactions must be performed behind a blast shield. After 24 h, the reactors were slowly cooled to room temperature, then further cooled in an ice bath for 15 min to condense any residual vapors before venting. Contents were diluted with dry diethyl ether (2 mL) and filtered through Celite over glass wool. Filtrates were diluted to 5 mL in volumetric glassware with dry ether. Solutions were analyzed via gas chromatography-flame ionization detection (GC-FID). GC samples were prepared with 300 μL of the reaction sample, 12.5 μL of 1,4-dioxane as internal standard, and diluted with dry ether to 1.5 mL. Yields and conversion were determined via standardization of the integral of the signal intensity to the internal standard and compared to independently prepared calibration curves for each individual product (i.e., ethanol, butanol, 2-ethylbutanol, etc.).

ASSOCIATED CONTENT

Supporting Information

The Supporting Information is available free of charge at https://pubs.acs.org/doi/10.1021/acsami.3c07396.

Experimental procedures, XPS, ICP−MS, and higher alcohols breakdown (PDF)

AUTHOR INFORMATION

Corresponding Authors

Paul A. Maggard − *Department of Chemistry, North Carolina State University, Raleigh, North Carolina 27695, United States;* orcid.org/0000-0002-3909-1590; Email: pamaggar@ncsu.edu

Karen I. Goldberg − *Department of Chemistry, University of Pennsylvania, Philadelphia, Pennsylvania 19104, United States;* orcid.org/0000-0002-0124-1709; Email: kig@sas.upenn.edu

Authors

Sabrine M. Cypher − *Department of Chemistry, University of Pennsylvania, Philadelphia, Pennsylvania 19104, United States;* orcid.org/0000-0002-4810-1180

Magnus Pauly − *Department of Chemistry, North Carolina State University, Raleigh, North Carolina 27695, United States*

Leslie G. Castro − *Department of Chemistry, University of Pennsylvania, Philadelphia, Pennsylvania 19104, United States*

Carrie L. Donley − *Chapel Hill Analytical and Nanofabrication Laboratory, Department of Chemistry, University of North Carolina, Chapel Hill, North Carolina 27599, United States;* orcid.org/0000-0003-0906-306X

Complete contact information is available at: https://pubs.acs.org/10.1021/acsami.3c07396

Notes

The authors declare no competing financial interest.

ACKNOWLEDGMENTS

This material is based upon work primarily supported as part of the Center for Hybrid Approaches in Solar Energy to Liquid Fuels (CHASE), an Energy Innovation Hub funded by the U.S. Department of Energy, Office of Science, Office of Basic Energy Sciences, under award no. DE-SC0021173. This work made use of instrumentation (XPS) at the Chapel Hill Analytical and Nanofabrication Laboratory, CHANL, a member of the North Carolina Research Triangle Nanotechnology Network, RTNN, which is supported by the National Science Foundation, grant ECCS-2025064, as part of the National Nanotechnology Coordinated Infrastructure, NNCI. Leslie Castro acknowledges the National Science Foundation-funded Research Experience for Undergraduates program under award no NSF-1851640. We would also like to acknowledge Dr. Marina Sokolsky-Papkov and Nanomedicines Characterization Core (NCore) of the UNC Eshelman School of Pharmacy and UNC School of Medicine for their assistance with ICP−MS analysis.

REFERENCES

(1) Pandey, A.; Larroche, C.; Ricke, S.; Dussap, C.-G.; Gnansounou, E. *Biofuels, Alternative Feedstocks, and Conversion Processes*, 1st ed.; Academic Press, 2011.

(2) Xu, H.; Rebollar, D.; He, H.; Chong, L.; Liu, Y.; Liu, C.; Sun, C.-J.; Li, T.; Muntean, J. V.; Winans, R. E.; Liu, D.-J.; Xu, T. Highly Selective Electrocatalytic CO_2 Reduction to Ethanol by Metallic Clusters Dynamically Formed from Atomically Dispersed Copper. *Nat. Energy* **2020**, *5*, 623−632.

(3) Hahn, C.; Hatsukade, T.; Kim, Y.-G.; Vailionis, A.; Baricuatro, J. H.; Higgins, D. C.; Nitopi, S. A.; Soriaga, M. P.; Jaramillo, T. F. Engineering Cu surfaces for the electrocatalytic conversion of CO_2: Controlling selectivity toward oxygenates and hydrocarbons. *Proc. Natl. Acad. Sci.* **2017**, *114*, 5918−5923.

(4) Specific energy and energy density of fuels. https://neutrium.net/properties/specific-energy-and-energy-density-of-fuels/ (accessed Dec 6, 2021).

(5) Swana, J.; Yang, Y.; Behnam, M.; Thompson, R. An Analysis of Net Energy Production and Feedstock Availability for Biobutanol and Bioethanol. *Bioresour. Technol.* **2011**, *102*, 2112−2117.

(6) Singh, S. B.; Dhar, A.; Agarwal, A. K. Technical Feasibility Study of Butanol−Gasoline Blends for Powering Medium-Duty Transportation Spark Ignition Engine. *Renewable Energy* **2015**, *76*, 706−716.

(7) Dürre, P. Biobutanol: An Attractive Biofuel. *Biotechnol. J.* **2007**, *2*, 1525−1534.
(8) Harvey, B. G.; Meylemans, H. A. The Role of Butanol in the Development of Sustainable Fuel Technologies. *J. Chem. Technol. Biotechnol.* **2011**, *86*, 2−9.
(9) Miers, S. A.; Carlson, R. W.; McConnell, S. S.; Ng, H. K.; Wallner, T.; Esper, J. L. Drive Cycle Analysis of Butanol/Diesel Blends in a Light-Duty Vehicle. *SAE Technical Paper*, 2008. 2008-01-2381.
(10) U.S. Energy Information Administration. Almost all U.S. gasoline is blended with 10% ethanol. https://www.eia.gov/todayinenergy/detail.php?id=26092 (accessed March 28, 2022).
(11) Xue, C.; Zhao, X.-Q.; Liu, C.-G.; Chen, L.-J.; Bai, F.-W. Prospective and Development of Butanol as an Advanced Biofuel. *Biotechnol. Adv.* **2013**, *31*, 1575−1584.
(12) Guerbet, M. Action Des Alcools Ethylique, Isobutylique, Isoamylique Sur Leurs Derives Sodes. *C. R. Acad. Sci. Ser.* **1899**, *128*, 1002−1004.
(13) Guerbet, M. M. C. R. Condensation de l'alcool Isoproyplique Avec Son Derive Sode; Formation Du Methylisobutylcarbinol et Du Dimethyl-2,4-Heptanol-6. *Comptes Rendus* **1909**, *149*, 129−132.
(14) Veibel, S.; Nielsen, J. I. On the Mechanism of the Guerbet Reaction. *Tetrahedron* **1967**, *23*, 1723−1733.
(15) Choi, H.; Han, J.; Lee, J. Renewable Butanol Production via Catalytic Routes. *Int. J. Environ. Res. Publ. Health* **2021**, *18*, 11749.
(16) Das, K.; Yasmin, E.; Das, B.; Srivastava, H. K.; Kumar, A. Phosphine-Free Pincer-Ruthenium Catalyzed Biofuel Production: High Rates, Yields and Turnovers of Solventless Alcohol Alkylation. *Catal. Sci. Technol.* **2020**, *10*, 8347−8358.
(17) Koda, K.; Matsu-ura, T.; Obora, Y.; Ishii, Y. Guerbet Reaction of Ethanol to n-Butanol Catalyzed by Iridium Complexes. *Chem. Lett.* **2009**, *38*, 838−839.
(18) Chakraborty, S.; Piszel, P. E.; Hayes, C. E.; Baker, R. T.; Jones, W. D. Highly Selective Formation of n-Butanol from Ethanol through the Guerbet Process: A Tandem Catalytic Approach. *J. Am. Chem. Soc.* **2015**, *137*, 14264−14267.
(19) Wingad, R. L.; Gates, P. J.; Street, S. T. G.; Wass, D. F. Catalytic Conversion of Ethanol to n-Butanol Using Ruthenium P−N Ligand Complexes. *ACS Catal.* **2015**, *5*, 5822−5826.
(20) Tseng, K.-N. T.; Lin, S.; Kampf, J. W.; Szymczak, N. K. Upgrading Ethanol to 1-Butanol with a Homogeneous Air-Stable Ruthenium Catalyst. *Chem. Commun.* **2016**, *52*, 2901−2904.
(21) Xie, Y.; Ben-David, Y.; Shimon, L. J. W.; Milstein, D. Highly Efficient Process for Production of Biofuel from Ethanol Catalyzed by Ruthenium Pincer Complexes. *J. Am. Chem. Soc.* **2016**, *138*, 9077−9080.
(22) Kulkarni, N. V.; Brennessel, W. W.; Jones, W. D. Catalytic Upgrading of Ethanol to n-Butanol via Manganese-Mediated Guerbet Reaction. *ACS Catal.* **2018**, *8*, 997−1002.
(23) Rawat, K. S.; Mandal, S. C.; Bhauriyal, P.; Garg, P.; Pathak, B. Catalytic Upgrading of Ethanol to N-Butanol Using an Aliphatic Mn−PNP Complex: Theoretical Insights into Reaction Mechanisms and Product Selectivity. *Catal. Sci. Technol.* **2019**, *9*, 2794−2805.
(24) King, A. M.; Sparkes, H. A.; Wingad, R. L.; Wass, D. F. Manganese Diphosphine and Phosphinoamine Complexes Are Effective Catalysts for the Production of Biofuel Alcohols via the Guerbet Reaction. *Organometallics* **2020**, *39*, 3873−3878.
(25) DiBenedetto, T. A.; Jones, W. D. Upgrading of Ethanol to n-Butanol via a Ruthenium Catalyst in Aqueous Solution. *Organometallics* **2021**, *40*, 1884−1888.
(26) King, A. M.; Wingad, R. L.; Pridmore, N. E.; Pringle, P. G.; Wass, D. F. Rhenium Complexes Bearing Tridentate and Bidentate Phosphinoamine Ligands in the Production of Biofuel Alcohols via the Guerbet Reaction. *Organometallics* **2021**, *40*, 2844−2851.
(27) Davies, A. M.; Li, Z.-Y.; Stephenson, C. R. J.; Szymczak, N. K. Valorization of Ethanol: Ruthenium-Catalyzed Guerbet and Sequential Functionalization Processes. *ACS Catal.* **2022**, *12*, 6729−6736.
(28) Zhang, X.; Liu, Z.; Xu, X.; Yue, H.; Tian, G.; Feng, S. Hydrothermal Synthesis of 1-Butanol from Ethanol Catalyzed with Commercial Cobalt Powder. *ACS Sustain. Chem. Eng.* **2013**, *1*, 1493−1497.
(29) Zhang, J.; Shi, K.; Zhu, Y.; An, Z.; Wang, W.; Ma, X.; Shu, X.; Song, H.; Xiang, X.; He, J. Interfacial Sites in Ag Supported Layered Double Oxide for Dehydrogenation Coupling of Ethanol to n-Butanol. *ChemistryOpen* **2021**, *10*, 1095−1103.
(30) Li, S.; Han, X.; An, H.; Zhao, X.; Wang, Y. Improving the Catalytic Stability of Ni/TiO2 for Ethanol Guerbet Condensation: Influence of Second Metal Component. *Kinet. Catal.* **2021**, *62*, 632−640.
(31) Seekhiaw, P.; Pinthong, P.; Praserthdam, P.; Jongsomjit, B. Optimal Conditions for Butanol Production from Ethanol over MgAlO Catalyst Derived from Mg-Al Layer Double Hydroxides. *J. Oleo Sci.* **2022**, *71*, 141−149.
(32) Dziugan, P.; Jastrzabek, K. G.; Binczarski, M.; Karski, S.; Witonska, I. A.; Kolesinska, B.; Kaminski, Z. J. Continuous Catalytic Coupling of Raw Bioethanol into Butanol and Higher Homologues. *Fuel* **2015**, *158*, 81−90.
(33) Riittonen, T.; Toukoniitty, E.; Madnani, D. K.; Leino, A.-R.; Kordas, K.; Szabo, M.; Sapi, A.; Arve, K.; Wärnå, J.; Mikkola, J.-P. One-Pot Liquid-Phase Catalytic Conversion of Ethanol to 1-Butanol over Aluminium Oxide—The Effect of the Active Metal on the Selectivity. *Catalysts* **2012**, *2*, 68−84.
(34) Riittonen, T.; Eränen, K.; Mäki-Arvela, P.; Shchukarev, A.; Rautio, A.-R.; Kordas, K.; Kumar, N.; Salmi, T.; Mikkola, J.-P. Continuous Liquid-Phase Valorization of Bio-Ethanol Towards Bio-Butanol over Metal Modified Alumina. *Renewable Energy* **2015**, *74*, 369−378.
(35) Marcu, I.-C.; Tanchoux, N.; Fajula, F.; Tichit, D. Catalytic Conversion of Ethanol into Butanol over M−Mg−Al Mixed Oxide Catalysts (M = Pd, Ag, Mn, Fe, Cu, Sm, Yb) Obtained from LDH Precursors. *Catal. Lett.* **2013**, *143*, 23−30.
(36) Carvalho, D. L.; de Avillez, R. R.; Rodrigues, M. T.; Borges, L. E. P.; Appel, L. G. Mg and Al Mixed Oxides and the Synthesis of n-Butanol from Ethanol. *Appl. Catal., A* **2012**, *415*−*416*, 96−100.
(37) Neumann, C. N.; Rozeveld, S. J.; Yu, M.; Rieth, A. J.; Dincă, M. Metal−Organic Framework-Derived Guerbet Catalyst Effectively Differentiates between Ethanol and Butanol. *J. Am. Chem. Soc.* **2019**, *141*, 17477−17481.
(38) Wang, S.-C.; Cendejas, M. C.; Hermans, I. Insights into Ethanol Coupling over Hydroxyapatite using Modulation Excitation Operando Infrared Spectroscopy. *ChemCatChem* **2020**, *12*, 4167−4175.
(39) Xue, M.; Yang, B.; Xia, C.; Zhu, G. Upgrading Ethanol to Higher Alcohols via Biomass-Derived Ni/Bio-Apatite. *ACS Sustain. Chem. Eng.* **2022**, *10*, 3466−3476.
(40) Ramasamy, K. K.; Gray, M.; Job, H.; Santosa, D.; Li, X. S.; Devaraj, A.; Karkamkar, A.; Wang, Y. Role of Calcination Temperature on the Hydrotalcite Derived MgO−Al2O3 in Converting Ethanol to Butanol. *Top. Catal.* **2016**, *59*, 46−54.
(41) Das, K.; Kathuria, L.; Jasra, R. V.; Dhole, S.; Kumar, A. Microwave-Assisted Pincer-Ruthenium Catalyzed Guerbet Reaction for the Upgradation of Bio-Ethanol to Bio-Butanol. *Catal. Sci. Technol.* **2023**, *13*, 1763−1776.
(42) Pauly, M.; Kröger, J.; Duppel, V.; Murphey, C.; Cahoon, J.; Lotsch, B. V.; Maggard, P. A. Unveiling the Complex Configurational Landscape of the Intralayer Cavities in a Crystalline Carbon Nitride. *Chem. Sci.* **2022**, *13*, 3187−3193.
(43) Wang, Y.; Yao, J.; Li, H.; Su, D.; Antonietti, M. Highly Selective Hydrogenation of Phenol and Derivatives over a Pd@Carbon Nitride Catalyst in Aqueous Media. *J. Am. Chem. Soc.* **2011**, *133*, 2362−2365.
(44) Chen, Z.; Vorobyeva, E.; Mitchell, S.; Fako, E.; López, N.; Collins, S. M.; Leary, R. K.; Midgley, P. A.; Hauert, R.; Pérez-Ramírez, J. Single-Atom Heterogeneous Catalysts Based on Distinct Carbon Nitride Scaffolds. *Natl. Sci. Rev.* **2018**, *5*, 642−652.
(45) Sangwan, V. K.; Hersam, M. C. Electronic Transport in Two-Dimensional Materials. *Annu. Rev. Phys. Chem.* **2018**, *69*, 299−325.
(46) Liu, X.; Hersam, M. C. Interface Characterization and Control of 2D Materials and Heterostructures. *Adv. Mater.* **2018**, *30*, 1801586.

https://doi.org/10.1021/acsami.3c07396
ACS Appl. Mater. Interfaces 2023, 15, 36384−36393

(47) Shin, Y.; Just-Baringo, X.; Zarattini, M.; Isherwood, L. H.; Baidak, A.; Kostarelos, K.; Larrosa, I.; Casiraghi, C. Charge-Tunable Graphene Dispersions in Water Made with Amphoteric Pyrene Derivatives. *Mol. Syst. Des. Eng.* **2019**, *4*, 503−510.
(48) Li, D. O.; Gilliam, M. S.; Chu, X. S.; Yousaf, A.; Guo, Y.; Green, A. A.; Wang, Q. H. Covalent Chemical Functionalization of Semiconducting Layered Chalcogenide Nanosheets. *Mol. Syst. Des. Eng.* **2019**, *4*, 962−973.
(49) Kasap, H.; Caputo, C. A.; Martindale, B. C. M.; Godin, R.; Lau, V. W.-h.; Lotsch, B. V.; Durrant, J. R.; Reisner, E. Solar-Driven Reduction of Aqueous Protons Coupled to Selective Alcohol Oxidation with a Carbon Nitride−Molecular Ni Catalyst System. *J. Am. Chem. Soc.* **2016**, *138*, 9183−9192.
(50) Cai, Y.; Tang, Y.; Fan, L.; Lefebvre, Q.; Hou, H.; Rueping, M. Heterogeneous Visible-Light Photoredox Catalysis with Graphitic Carbon Nitride for α-Aminoalkyl Radical Additions, Allylations, and Heteroarylations. *ACS Catal.* **2018**, *8*, 9471−9476.
(51) Heymann, L.; Bittinger, S. C.; Klinke, C. Molecular Doping of Electrochemically Prepared Triazine-Based Carbon Nitride by 2,4,6-Triaminopyrimidine for Improved Photocatalytic Properties. *ACS Omega* **2018**, *3*, 17042−17048.
(52) Chen, C.-H.; Chang, K.-S. Fabrication and Photodegradation Application of Isopropanol-Functionalized Poly (Triazine Imide). *J. Electron. Mater.* **2020**, *49*, 1518−1526.
(53) Jia, X.; Guan, Q.; Chen, Y.; Wang, Y.; Zhao, Q.; Li, J. Poly (triazine imide) (PTI) and Graphene Hybrids Supported PtSn Catalysts for Enhanced Electrocatalytic Oxidation of Ethanol. *Appl. Surf. Sci.* **2019**, *492*, 879−885.
(54) The Tishchenko (Lewis acid-catalyzed) and Cannizzaro (base-catalyzed) reactions are known side reactions for the Guerbet reaction. The main products of these reactions are ethyl acetate or acetate salts. Ethyl acetate was observed only in trace amounts in the product mixture, and no sodium acetate was observed at all. These side reactions were not responsible for the missing ethanol seen.
(55) Neumann, C. N.; Rozeveld, S. J.; Dincă, M. MOF-Derived RuCo Catalyzes the Formation of a Plasticizer Alcohol from Renewable Precursors. *ACS Catal.* **2021**, *11*, 8521−8526.
(56) A white precipitate in product solutions formed when left undisturbed overnight which could be consistent with butyrate formation,[65] but the precipitate could not be definitely characterized. The precipitate was not soluble in benzene-d_6 or chloroform-*d* when ^{1}H NMR spectroscopy was attempted.
(57) Nieto, I.; Livings, M. S.; Sacci, J. B.; Reuther, L. E.; Zeller, M.; Papish, E. T. Transfer Hydrogenation in Water via a Ruthenium Catalyst with OH Groups near the Metal Center on a bipy Scaffold. *Organometallics* **2011**, *30*, 6339−6342.
(58) Hao, W.; Joe, C. L.; Ayers, S.; Darù, A.; Daley, R. A.; Domanski, M.; Chen, J. S.; Schmidt, M. A.; Blackmond, D. G. Ru-Catalyzed Enantioselective Hydrogenation of 2-Pyridyl-Substituted Alkenes and Substrate-Mediated H/D Exchange. *ACS Catal.* **2022**, *12*, 1150−1160.
(59) Sheludko, B.; Cunningham, M. T.; Goldman, A. S.; Celik, F. E. Continuous-Flow Alkane Dehydrogenation by Supported Pincer-Ligated Iridium Catalysts at Elevated Temperatures. *ACS Catal.* **2018**, *8*, 7828−7841.
(60) Wu, Y.; Hu, G.; Rooney, C. L.; Brudvig, G. W.; Wang, H. Heterogeneous Nature of Electrocatalytic CO/CO2 Reduction by Cobalt Phthalocyanines. *ChemSusChem* **2020**, *13*, 6296−6299.
(61) Jackson, M. N.; Surendranath, Y. Molecular Control of Heterogeneous Electrocatalysis through Graphite Conjugation. *Acc. Chem. Res.* **2019**, *52*, 3432−3441.
(62) Muratsugu, S.; Maity, N.; Baba, H.; Tasaki, M.; Tada, M. Preparation and Catalytic Performance of a Molecularly Imprinted Pd Complex Catalyst for Suzuki Cross-Coupling Reactions. *Dalton Trans.* **2017**, *46*, 3125−3134.
(63) Moulder, J. F.; Stickle, W. F.; Sobol, P. E.; Bomben, K. D. *Handbook of X-ray Photoelectron Spectroscopy: A Reference Book of Standard Data for Use in X-ray Photoelectron Spectroscopy*; Physical Electronics, Inc.: Eden Prairie, MN, 1995.
(64) Luo, N.; Zhong, Y.; Wen, H.; Luo, R. Cyclometalated Iridium Complex-Catalyzed N-Alkylation of Amines with Alcohols via Borrowing Hydrogen in Aqueous Media. *ACS Omega* **2020**, *5*, 27723−27732.
(65) Zhang, C.; Liang, Q.; Yang, W.; Zhang, G.; Hu, M.; Zhang, G. Nickel(I)-Catalyzed (De)Hydrogenative Coupling of Amines and Alkyl Heteroarenes With Alcohols. *Green Chem.* **2022**, *24*, 7368−7375.
(66) Zhang, Q.; Dong, J.; Liu, Y.; Wang, Y.; Cao, Y. Towards a Green Bulk-Scale Biobutanol from Bioethanol Upgrading. *J. Energy Chem.* **2016**, *25*, 907−910.
(67) Burness, D. M. Methyl 3-Methyl-2-Furoate. *Org. Synth.* **1959**, *39*, 49−52.
(68) Under an inert atmosphere, dry benzene (20 mL) and methanol (0.4 mL) were added to a dried Schlenk flask. Under active N_2 flow, sodium metal (4 small flakes) was added to the solution. A white precipitate formed immediately. It was stirred under an inert atmosphere until reaction ceased bubbling, cooled to room temperature, and all solid sodium has been reacted. The volatiles were removed on a rotary evaporator, and the solid was dried in vacuo for 2 days.
(69) White, C.; Yates, A.; Maitlis, P. M.; Heinekey, D. M. (η5-Pentamethylcyclopentadienyl)Rhodium and -Iridium Compounds. *Inorg. Synth.* **1992**, *29*, 228−234.
(70) Bennett, M. A.; Huang, T.-N.; Matheson, T. W.; Smith, A. K.; Ittel, S.; Nickerson, W. (η6-Hexamethylbenzene)Ruthenium Complexes. *Inorganic Syntheses*; Wiley Online Library, 1982; Vol. *21*, pp 74−78.

https://doi.org/10.1021/acsami.3c07396
ACS Appl. Mater. Interfaces 2023, 15, 36384−36393